Peel and Shear Fracture Characterization of Debonding in FRP Plated Concrete Affected by Moisture

Ching Au, A.M.ASCE[1]; and Oral Büyüköztürk, M.ASCE[2]

Abstract: The objective of this paper is to develop a new mechanistic understanding of moisture affected debonding failures in carbon fiber reinforced polymer (CFRP) plated concrete systems by mechanically testing accelerated moisture conditioned mesoscale peel and shear interface fracture specimens. Central to the investigation is the use of interface fracture toughness as the quantification parameter of the CFRP-epoxy-concrete trilayer system, which is considered a bond property, to analyze, compare, and correlate physical observations. Results have shown that fracture toughness of the CFRP bonded concrete systems significantly degrades, and its value becomes asymptotic with increasing moisture ingress. This asymptotic behavior is associated with certain moisture concentration levels as predicted by a three-dimensional moisture diffusion simulation. The generally observed debonding mode by concrete delamination for the dry specimens changes to an epoxy/concrete interface separation mode for the wet specimens. Finite element fracture computation, mixed-mode characterization, and kink criterion implementation synergistically suggest that the interface separation mode is attributed to an interfacial material toughening and an interface weakening mechanism as a consequence of moisture diffusion.

DOI: 10.1061/(ASCE)1090-0268(2006)10:1(35)

CE Database subject headings: Concrete beams; Cracking; Bonding; Diffusion; Fracture; Fiber reinforced polymers; Interfaces; Moisture; Shear.

Background

Fiber reinforced polymer (FRP) materials are now broadly consumed in civil infrastructure applications for flexural strengthening of reinforced concrete (RC) beam and slab elements. Lightweight FRP laminates in the form of strips and sheets are often bonded to the soffits of these RC elements using a thixotropic ambient-cured epoxy that is designed for in situ overhead applications. Empirical results from short-term tests of FRP retrofitted concrete structures have shown that under many circumstances (including different loading type, material variations, and retrofit methods), concrete substrate debonding is the predominant mode of failure. For a beam system, concrete debonding, which is often brittle, can occur with little or no visible warning at load levels significantly lower than the expected flexural or shear strength of the retrofit system (Büyüköztürk and Hearing 1998). Delamination of the FRP laminate is also seen from time to time when relatively viscous adhesive is being used. These empirical observations have been reported by a number of research teams who worked at the structural scale (Kaiser 1989; Saadatmanesh and Ehsani 1990, 1991; Ritchie et al. 1991; Sharif et al. 1994; Büyüköztürk et al. 2004). A number of attempts have since been made to look at such debonding phenomena at a smaller scale using various physical models, such as the peel and lap shear specimens (Chajes et al. 1996; Taljsten 1997; Karbhari et al. 1997; Neubauer and Rostasy 1997; Bizindavyi and Neale 1999; Kimpara et al. 1999; Chen and Teng 2001; Nakaba et al. 2001; Wu et al. 2002; Gao et al. 2003) and various strength and debonding models have been suggested (Smith and Teng 2001). While the majority of these models are strength based, an increasing number of fracture-based models have recently been developed. Boyajian et al. (2005) devised a single contoured-cantilever beam specimen to facilitate Mode I fracture characterization of carbon FRP (CFRP)-concrete interfaces under various environmental conditions. This specimen is derived from the conventional double-cantilever beam (DCB) but only employs a single contoured arm such that a constant compliance gradient is attained for the particular layered-material system for convenient fracture toughness computation. Qiao and Xu (2004), on the other hand, developed a notched three-point bending beam that employs a fictitious crack model-based approach to characterize Mode I fracture of FRP-concrete bonded interfaces. It was found from this model that the interface fracture energy is not strongly dependent on the loading rates but increases with increasing epoxy curing time. Wan et al. (2004) attempted to assess the mixed-mode fracture energy by means of crack opening displacement (COD) measurement using computer vision on a modified DCB specimens. COD measurements suggested that the crack growth is predominantly Mode I, with a small Mode II component.

At the structural level, debonding is often found to initiate from the laminate ends where abrupt discontinuities result in high stress concentrations. Various methods of anchorages, such as anchor bolts, L-shaped plates, and U-anchors, have since been devised with varying levels of success to prevent debonding from happening (Sharif et al. 1994; Garden and Holloway 1998;

[1]PhD Candidate, Dept. of Civil and Environmental Engineering, Massachusetts Institute of Technology, Cambridge, MA 02139.

[2]Professor, Dept. of Civil and Environmental Engineering, Massachusetts Institute of Technology, Cambridge, MA 02139.

Note. Discussion open until July 1, 2006. Separate discussions must be submitted for individual papers. To extend the closing date by one month, a written request must be filed with the ASCE Managing Editor. The manuscript for this paper was submitted for review and possible publication on January 4, 2005; approved on July 14, 2005. This paper is part of the ***Journal of Composites for Construction***, Vol. 10, No. 1, February 1, 2006. ©ASCE, ISSN 1090-0268/2006/1-35–47/$25.00.

Khalifa et al. 1998; Khalifa and Nanni 2000; Smith and Teng 2001; Gunes 2004).

When sufficient and proper end anchorages are deployed, interface debonding would, however, be forced to take place elsewhere, often within the retrofitted span (Hassanen and Raoof 2001). Debonding within the retrofitted span is often initiated from flexural cracks and/or flexural-shear cracks where differential crack mouth movements occur when an external load is applied to the beam system. Such debonding initiation and propagation has been observed in a number of research studies (Kaiser 1989; Meier 1992; Neubauer and Rostasy 1997; Hearing 2000; Gunes 2004).

While the problem of debonding under short-term effects has been quite extensively studied, research regarding the durability of debonding has been very limited. A recent experimental work (Grace 2004) showed that structural performance of FRP retrofitted systems could be significantly impeded due to the introduction of various environmental effects, and that debonding in the FRP/concrete interface region plays a major role in such premature failures. In particular, the moisture effect has been identified as an important environmental deterioration mechanism promoting premature system failures. Grace (2004) conducted an array of tests on 78 large-scale retrofitted RC beams using CFRP plates and fabrics that were subjected to various environmental effects, including water, saltwater, freeze-thaw, dry heat, and alkalinity. After 10,000 h of respective continuous exposure, it was concluded that moisture could do the most damage in terms of ultimate beam strength, resulting in a 30% and 10% respective reduction for CFRP plate and CFRP sheet bonded beams. Debonding was observed as the primary failure mode, although details of such failures were not described explicitly.

The findings in that investigation regarding the detrimental effect of moisture were in line with other limited number of independent studies conducted on FRP retrofitted concrete beams, either with or without rebars, that were subjected to accelerated wet/dry cycles. Reduction in ultimate strength and stiffness due to such cycling was generally observed. Chajes et al. (1995) showed a 36% decrease in ultimate strength for glass FRP (GFRP) retrofitted specimens that were subjected to 100 wet/dry cycles, while a 19% reduction was shown for CFRP bonded specimens. Toutanji and Gomez (1997), on the other hand, observed a strength reduction that ranged from 3 to 33% on specimens made of various epoxy and FRP systems that were subjected to 300 wet/dry cycles in salt water. Failure was reported as a debonding mode that generally took place near the FRP/concrete interface. Mukhopadhyaya et al. (1998) found similar degradation trends on GFRP double-lap shear specimens that were subjected to comparable wet/dry conditioning. Karbhari and Zhao (1998) observed microcracking in the GFRP laminate in retrofitted cement mortar beams that were mechanically tested to failure under a four-point bend configuration. After 120 days of continuous moisture exposure, a 40% reduction in flexural strength was observed.

Research Objective and Approach

While previous studies have identified the detrimental role of moisture in FRP retrofitted systems, the debonding mechanics is presently not well understood due in part to the inherently less explicit strength-based approach in studying and quantifying the debonding phenomenon, which is by nature an interface fracture problem. Yet, moisture affected debonding has been shown to be a complex phenomenon that may involve material decohesion and/or interface separation. Unlike material decohesion (e.g., concrete delamination) of which debonding failure occurs as a result of material limits being utilized, interface separation is a debonding mode that is governed by the adhesion property of the adjoining constituent materials such that constituent material limits are not necessarily attained. While the strength approach may be capable of quantifying and analyzing material decohesion type of debonding, it intrinsically lacks the ability to describe adhesion related phenomenon.

The objective of this study is to develop an in-depth mechanistic understanding through the proper quantification of moisture affected debonding in CFRP plated concrete by means of an interface fracture approach that makes use of the interface fracture toughness, Γ, as the debonding quantification parameter, which is considered a bond property of the multilayer material system. This approach is considered particularly robust due to the fact that the bond property is assessed on bond lines of the real scale that can be replicated in laboratory settings using mesoscale interface fracture specimens. The toughness parameter is computed from a linear elastic fracture energy release rate model (G model) developed in parallel with this study (Au 2004; IST 2004) by the writers that is capable of describing the trilayer material debonding problem explicitly under a wide range of loading configurations. The use of such a linear model is justified by observations from our preliminary tests suggesting that wet specimens fracturing under peel and shear configurations demonstrate a slight overall nonlinearity because the fracture problem is more of an adhesion type, and does not necessarily involve the attainment of material limits. This aspect may need to be further evaluated; the present work aims at the development and application of a rigorous approach to study this complex fracture problem, and represents an exploratory effort.

For CFRP plated concrete, three materials (FRP, adhesive, and concrete) and two interfaces (FRP/adhesive and adhesive/concrete) are involved. Thus, in theory, five distinct debonding modes are possible. They are, namely, (1) FRP delamination; (2) FRP/adhesive separation; (3) adhesive decohesion; (4) adhesive/concrete separation; and (5) concrete substrate fracture. These five failure modes can be broadly classified as two classes of failure: material decohesion, and interface fracture. Failure modes (1), (3), and (5) are considered material decohesion, while failure modes (2) and (4) are considered interface fracture. With these debonding cases defined, each debonding mode can be described and quantified.

This study focuses on the characterization of debonding that is initiated from within the retrofit span as a result of differential crack mouth movement. The loading condition in the debonding vicinity is represented by means of a peel and a shear configuration as the limiting cases. Fig. 1 shows actual debonding configuration in a retrofitted beam and the fracture models selected for this study.

These two specimen configurations share the commonality of being a layered material system with the CFRP plate exposed on one side, closely resembling the realistic debonding problem at the structural scale. They also retain realistic bond line features (both width and thickness) of the bonded system at the mesoscale, which can be manufactured with relative ease in large quantities, and offer excellent test control.

Debonding characterization is conducted using these mesoscale peel and shear fracture models that are subjected to accelerated moisture conditioning to achieve various levels of moisture content in the bond region. They are then mechanically tested at

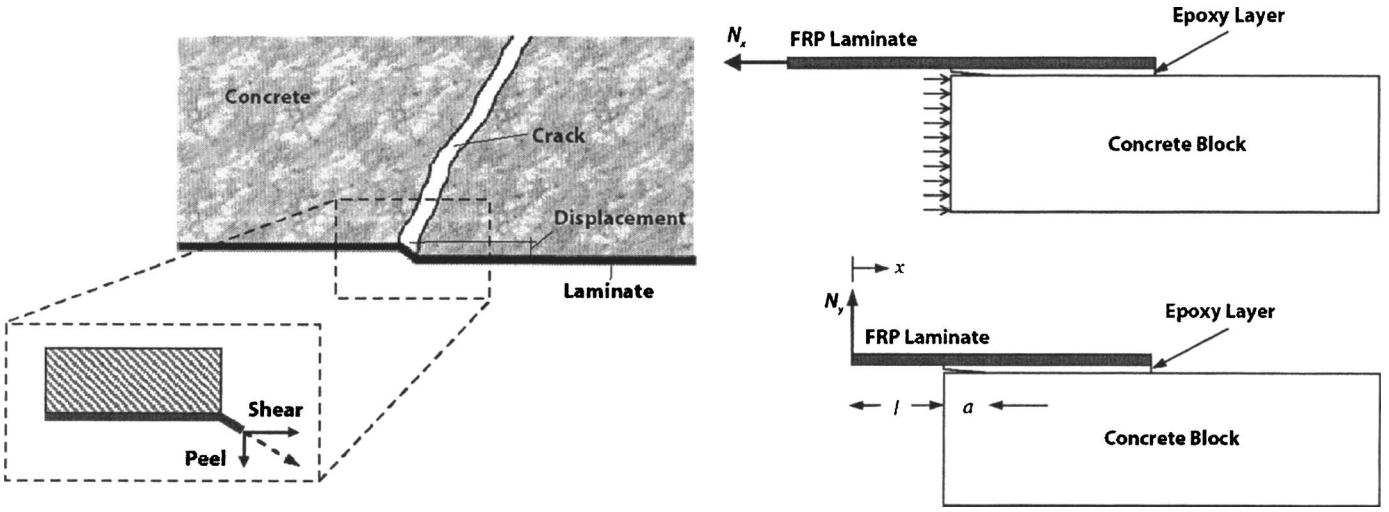

Fig. 1. Actual debonding configuration and selected fracture models

selected time intervals for capturing the change in bond property and debonding mode with respect to increasing moisture concentration, which is evaluated by means of three-dimensional (3D) moisture diffusion simulations (Au 2004). Diffusion and mechanical properties of the constituent materials, as a function of moisture uptake, are physically determined to act as inputs in the diffusion simulation and in the computation of toughness values. The knowledge of computed toughness values, simulated diffusion behavior, and observed debonding modes, combined with finite element fracture computation, mixed-mode characterization, and kink criterion implementation, form a synergistic analysis of the mechanistic debonding behavior affected by moisture. Readers should refer to Au (2004) and IST (2004) for details of the finite element moisture diffusion simulation, interface fracture computation, and mode separation computation.

Materials

The materials used in making the fracture specimens include a normal grade concrete, one type of CFRP plate, and one type of epoxy adhesive system. Concrete was composed of water, cement, sand, and gravel with a mass ratio of 0.5:1.0:2.4:1.6. Aggregates were carefully sieved and remixed to conform to the ASTM C33 grading standard. The maximum gravel size was set at 9.5 mm (3/8 in.) to meet the ASTM C192 requirement of it being three times smaller than the minimum specimen dimension. All aggregates that passed through sieve No. 100 were considered too fine and were discarded in order to meet the designed water-cement ratio while maintaining good workability. The fineness modulus of the remixed aggregates was determined to be 2.82. The mixing, casting, and curing procedures fully conformed to the stipulations set forth in ASTM C192. A 28-day curing schedule was followed. To ensure consistency, all concrete was produced from the same batch of mix on the same day, cast upright with the to-be-bonded surface in contact with the mold bottom, and subjected to the same 28-day curing schedule followed by oven drying prior to bonding. Drying of the concrete was ensured by no further weight change on 1-day intervals for 3 consecutive days. The 28-day and oven-dried compressive strengths are, respectively, 29.0 and 32.4 MPa; elastic modulus 21.8 and 26.2 GPa; and fracture toughness, 0.61 MPa$\sqrt{\text{m}}$ (or 17.1 J/m^2) and 0.82 MPa$\sqrt{\text{m}}$ (or 25.7 J/m^2).

CFRP laminates were obtained from a U.S. manufacturer. The laminates were in the form of continuous pultruded prepregnated plates that consisted of unidirectional carbon fibers embedded in an epoxy resin matrix. The fiber volumetric content was 68%. The plate thickness was measured at 1.28 mm. The CFRP plates were designed for strengthening concrete and timber, as well as masonry members, by bonding onto the structure as external reinforcements that are extensively used in retrofit applications. The laminates were fully cured and nonreactive. The plates were trimmed to size from the same roll of material using an identical sawing setup for each cut. The elastic modulus and tensile strength were experimentally determined as 148 and 2.7 GPa, respectively.

The epoxy adhesive that was obtained from a U.S. manufacturer was a structural adhesive system that was a two-component solvent-free epoxy material designed for use in vertical and overhead applications. Component A was an epoxy resin with elastomer additives, while Component B was an amine hardener. Both components contained fumed silica for thixotropy purposes. The mix ratio A:B was 100:25 by weight or 100:30 by volume. Mixing required a low-speed mixer at 400–600 rpm for 5 min until components were fully dispersed. The resulting mix was a beige-colored epoxy paste. Curing required 7 days in ambient environment. The mix procedure was strictly controlled to ensure consistency. The elastic modulus and tensile strength were experimentally determined as 1.5 and 23.0 MPa, respectively.

For the details of the moisture degraded material properties, the reader is referred to Au (2004) and IST (2004).

Interface Fracture Specimens

Both peel and shear fracture models were made of identical materials using identical sample preparation procedures. All models consisted of a 1.28 mm thick CFRP plate bonded to a 37.5-mm thick concrete block with a 1.0-mm thick epoxy bond line. Uniformity of the bond line thickness was controlled by a number of Teflon spacers surrounding the bond. The thickness values resembled that of a real CFRP retrofitted concrete bond. The width

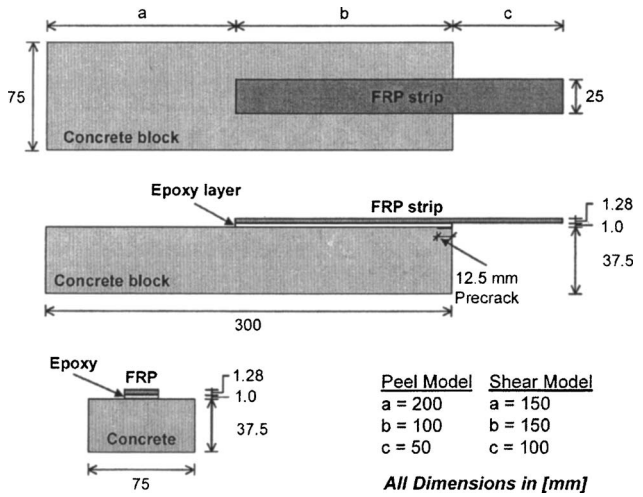

Fig. 2. Interface fracture specimen configurations

of the CFRP plate was 25 mm, and so was the width of the bond. The bond length of the peel model was 100 mm, while that of the shear model was 150 mm, which was chosen as the effective shear transfer length of the bond as determined from preliminary tests. The CFRP plate was centered along the longitudinal axis of the concrete block and a 25-mm shoulder was left on either side of the bond to remove edge effects, making the concrete block 75 mm wide in total. The cantilever length of the CFRP for the peel model was 50 mm, while that for the shear model was 100 mm so as to provide proper nonslip gripping according to the results of preliminary tests. A 12.5-mm precrack was introduced at the epoxy/concrete interface using an 80-micron thick Teflon tape. Note that the precrack location generally does not affect the final debonding location or mode because the crack always searches for the lowest-energy path for propagation. Fig. 2 illustrates a typical interface fracture specimen.

Oven-dried concrete blocks were subjected to a bond surface treatment of mechanical abrasion on the cast side that was in contact with the mold during casting by means of a pneumatic needle scaler. Mechanical abrasion was chosen over other means, such as water jetting, sanding, and grinding, because it has been determined (Chajes et al. 1996; Lorenzis et al. 2001; Toutanji and Ortiz 2001) that this method would provide maximum bond quality among all others. The concrete surfaces were roughened to a point that sound aggregates were exposed, and loosely held segregated particles were removed. Dust and debris were subsequently removed from the surface by compressed air, and cleaned by methyl ethyl ketone to ensure a sound adhesion surface prior to bonding.

Test Program

All specimens were divided into two main groups for regular and high-temperature moisture conditioning, respectively, at 23 and 50°C. Each temperature group consisted of the peel and shear test subgroups. Each subgroup was conditioned for 0, 2, 4, and 8 weeks. For each conditioning period, three randomly chosen samples were taken out, totaling 42 specimens mechanically tested to failure in standard laboratory conditions. Preliminary tests showed that while the variability of the interface fracture toughness can be great for dry specimens, such a variation for wet specimens is much smaller due to the nature of the wet material and adhesive behavior, as will be illustrated in subsequent sections. Hence, experiments on three samples per condition are considered to be sufficient to meet the objective of the test program. The selected time intervals were chosen based on the distinguishable moisture concentration patterns indicated from the results of a 3D moisture diffusion simulation by the finite element method using the exact specimen geometry and experimentally determined diffusion properties (Au 2004; IST 2004). Correspondence of the conditioning duration and the estimated normalized moisture concentration, C, (defined as moisture content at a given point in time divided by the saturated moisture content) in the epoxy/concrete bond interface are summarized in Table 1.

Table 1. Correspondence of Conditioning Duration and Normalized Concentration

Conditioning duration (weeks)	Estimated minimum C (%)
0	0
2	16
4	30
8	50

0-week conditioning corresponded to initial dry [defined as 50% relative humidity (RH)] testing without any moisture conditioning. Other specimens were conditioned at 100% RH at their respective temperatures. Continuous moisture conditioning represents an accelerated conditioning environment for both temperature groups.

High-temperature wet conditioning was conducted using a Q-Fog CCT 1100 (Cleveland) environmental chamber, while room-temperature wet conditioning was conducted in water baths in the laboratory with temperature control. All specimens were placed inside the conditioning chamber uniformly spaced to maximize moisture exposure and uniformity. The high-temperature conditioning represents a realistic upper bound of service temperature that could be reached in the soffit of a RC structural member (Mays and Hutchinson 1992).

Peel Fracture

Peel fracture tests were performed on an Instron (Norwood, Mass.) universal test machine using a 2.2 kN (500 lb) load cell under displacement control. Crosshead speed was chosen to be 2 mm/min such that the first peel crack advance took place within 5 min. All specimens were tested at standard laboratory condition. High-temperature conditioned specimens were removed from the conditioning chambers, wrapped in impermeable plastic wrap to retain moisture, and left for a few hours until the specimens reached the test temperature to prevent moisture desorption driven by temperature differential.

Each peel fracture specimen was rigidly clamped by a specially designed fixture, which was secured to the lower piston of the Instron. Alignment and leveling of the specimen were carefully performed using setscrews that were built into the fixture. The upper load cell was connected with a high carbon steel rod (Grade AISI 1055) designed with a 360° hinge mechanism on both ends to make the vertical peel possible. At all registered load levels, displacement within the rod was considered negligible due to low load. Load, crosshead displacement, and crack length were

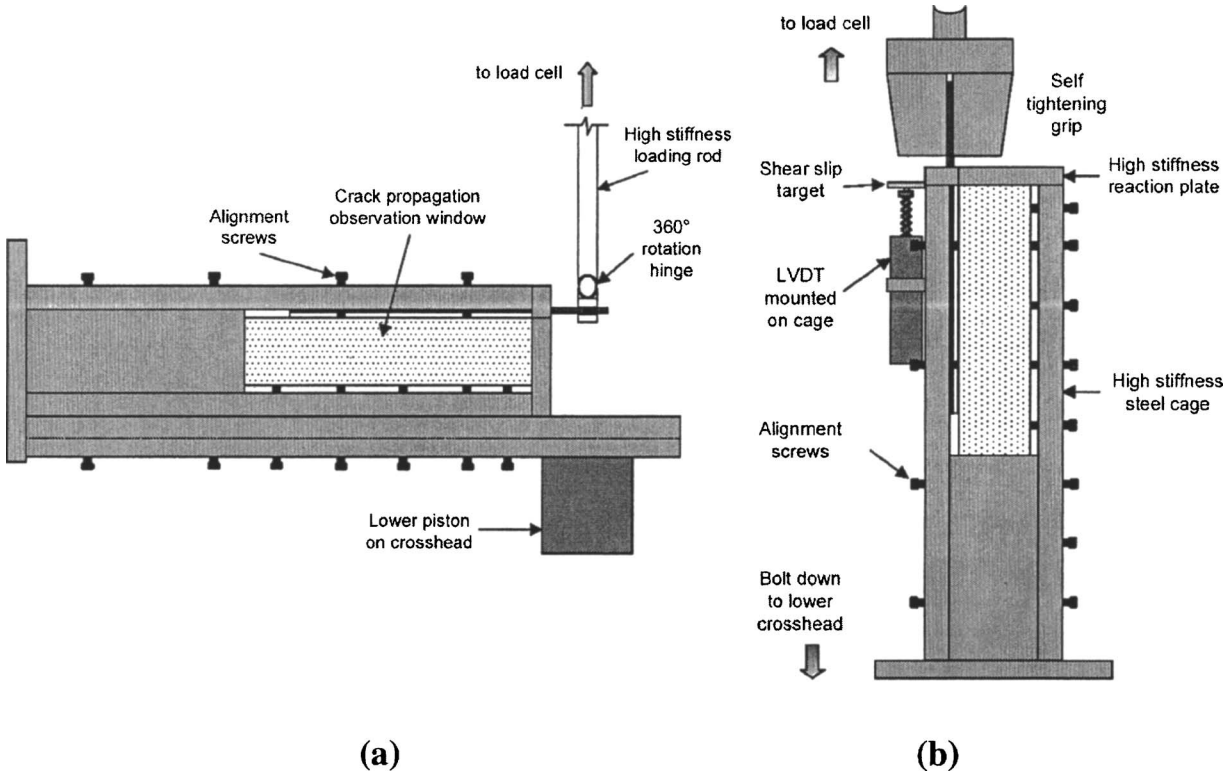

Fig. 3. (a) Peel fracture test setup and (b) shear fracture test setup

carefully and continuously monitored until the CFRP plate was entirely peeled off. The complete peel fracture setup is shown in Fig. 3(a).

Shear Fracture

Shear fracture tests were carried out in an upright position also in the same Instron universal test machine using a 50 kN load cell displacement controlled at 1 mm/min. Note that the crosshead speed for peel fracture was higher that that of shear fracture, because it needed to account for bending of the CFRP plate during the peeling process. All conditioned specimens were tested in standard laboratory conditions. Each shear fracture specimen was rigidly clamped in the specially designed carbon steel fixture (Grade AISI 1018), which was secured to the lower crosshead. A 12.5-mm thick reaction plate provided the necessary rigidity, after some preliminary testing, to prevent the concrete block from moving while the CFRP plate was pulled. Alignment was carefully adjusted so that the plate lined up with the longitudinal axis of the upper self-tightening serrated grip.

A 50-mm grip length was used to ensure no slippage under the range of critical load level. In fact, it has been preliminarily tested that the 25-mm wide CFRP plate exhibited no slippage up to the load cell limit, which was 50 kN, while the critical load level of the shear fracture specimens was less than one-half of that limit. Shear slip was measured by a linear variable displacement transducer to monitor the displacement of a 6-mm thick Plexiglass target that was adhered onto the CFRP plate right at the precrack tip location. The complete shear fracture test setup is shown in Fig. 3(b).

Results

Failure Modes

Peel Debonding Modes

Typical failure modes with and without moisture conditioning are shown in Fig. 4. All dry specimens failed by concrete delamination, rendering a material decohesion mode. The precrack, which was introduced at the epoxy/concrete interface, kinked into the concrete substrate near the epoxy/concrete interface on the first crack advance, and continued to fracture parallel to the interface

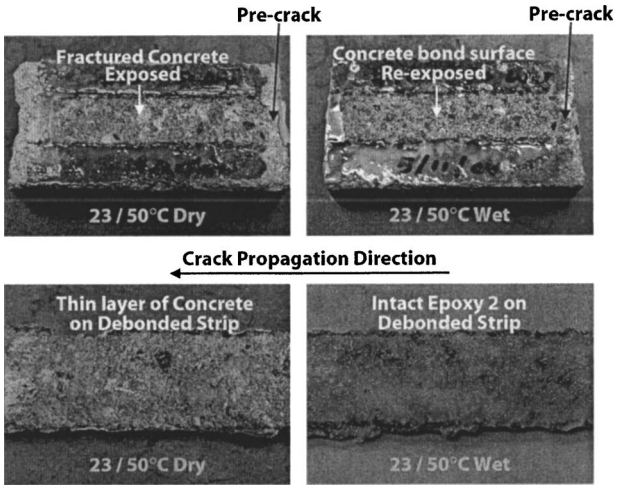

Fig. 4. Typical peel debonding modes

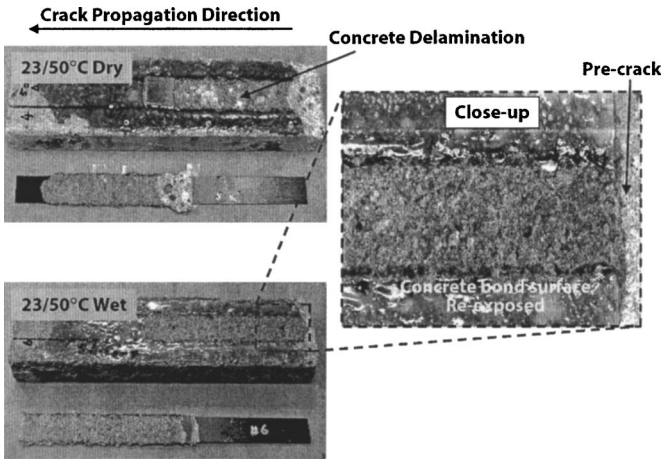

Fig. 5. Typical shear debonding modes

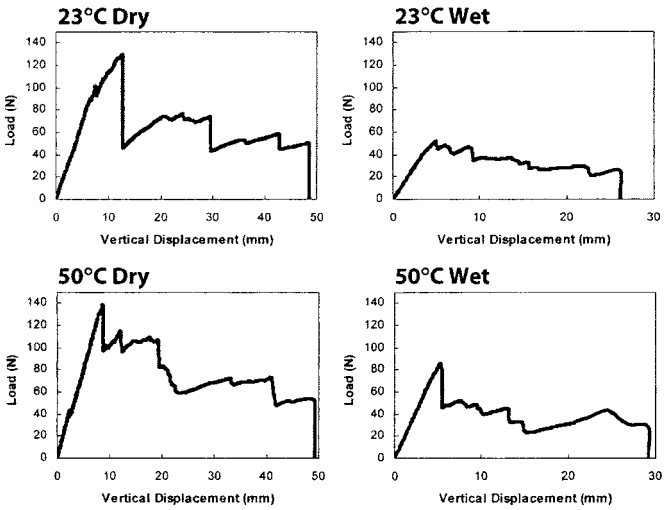

Fig. 6. Typical peel load-displacement curves

until complete peel off. A thin layer of concrete was found adhered to the debonded strip, which consisted of an intact adhesive layer.

Wet specimens, on the other hand, exhibited a distinctive epoxy/concrete interface separation. Only a relatively small amount of loose concrete particles adhered to the debonded plate, which consisted of the CFRP plate and an almost intact adhesive layer. The matching profile of the bond line was revealed from the adhesive side and the failure surfaces were still damp to the touch. The needle scaler-roughened concrete surface was once again revealed. While failure was observed as a crack-and-halt progressive phenomenon, it was noted that although the peel fracture process did not take place all at once for the whole strip, the crack did not kink into the concrete substrate at all during the whole process but remained propagating along the moist epoxy/concrete interface.

Shear Debonding Modes

In all shear failures, debonding occurred with a rapid propagation, as opposed to the crack-and-halt progressive manner. In general, shear fracture modes were identical to the peel counterparts. Fig. 5 shows the typical failure modes under shear load configurations. Concrete delamination was observed for dry specimens. Initially, a concrete chunk often sheared off in the vicinity of the reaction plate. The crack then kinked into the concrete near the epoxy/concrete interface and propagated parallel to that interface leading to failure in a concrete delamination mode.

Wet specimens exhibited an epoxy/concrete interface separation as in the peel case. The fractured interface was still damp to the touch and close-ups showed that the precrack concrete surface was at the same level as the freshly re-exposed concrete surface after debonding, confirming the observation of an interface separation mode. Exposed aggregates were still intact and the roughened surface profiles were very well preserved. Alignment markings were still clearly seen. Upon examination of the sheared surface, it was observed that the aggregates were not sheared off.

Load-Displacement Behavior

Peel Debonding Behavior

Typical load-displacement curves for peel fracture specimens before and after moisture conditioning are shown in Fig. 6. It is observed that a typical load-displacement curve produced by a peel test appeared in a seesaw pattern with decreasing local peak loads as the crack propagated further. Each local peak represented the onset of crack advance and the sudden drop in load corresponded to the actual crack front propagation. The first peak was always the highest, signifying a larger fracture resistance to overcome, possibly due to the blunter crack tip that was introduced by the edge of a Teflon tape. Subsequent crack fronts were sharper as they naturally evolved, amplifying the crack intensity in the tip vicinity. Unloading and reloading curves that followed instantaneous load drops were, in general, secant lines that radiated from the origin. This is an important observation as it means that the peel fracture process was globally linear elastic, and the strain energy built up by the peel force just before the onset of crack advance was fully exhausted at crack advance. The difference between dry and wet specimens with regard to load-displacement behavior was that dry specimens generally exhibited higher peak loads, as well as sharper drop in load upon crack advance.

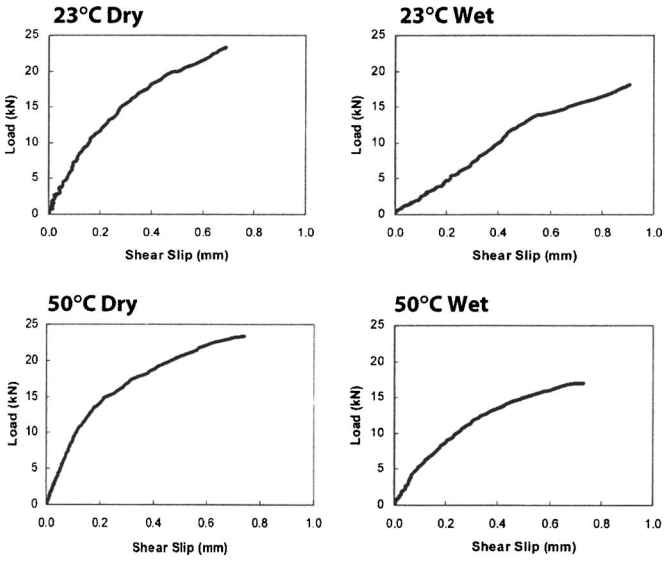

Fig. 7. Typical shear load-displacement curves

Table 2. A_1 and I_1

Case	A_1	I_1
1	Σ_{13}	$\frac{\Sigma_{13}}{12}$
2	$\Sigma_{13}+\Sigma_{23}\frac{\gamma}{\eta}$	$\Sigma_{13}\left[\left(\frac{\gamma}{\eta}\right)^2+(1-2\delta)\left(\frac{\gamma}{\eta}\right)+\frac{3(1-2\delta)^2+1}{12}\right]+\Sigma_{23}\left[\delta\left(\frac{\gamma}{\eta}\right)\left(\delta-\frac{\gamma}{\eta}\right)+\frac{1}{3}\left(\frac{\gamma}{\eta}\right)^3\right]$
3	$\Sigma_{13}(1-\xi_1)$	$\Sigma_{13}\frac{(1-\xi_1)^3}{12}$
4	$\Sigma_{13}+\Sigma_{23}\left(\frac{\gamma}{\eta}-\xi_2\right)$	$\Sigma_{13}\left[\left(\frac{\gamma}{\eta}\right)^2+(1-2\Delta_2-2\xi_2)\left(\frac{\gamma}{\eta}\right)+\frac{3(1-2\Delta_2)^2+1}{12}+\xi_2^2-\xi_2(1-2\Delta_2)\right]$ $+\Sigma_{23}\left[\Delta_2\left(\frac{\gamma}{\eta}\right)\left(\Delta_2-\frac{\gamma}{\eta}\right)+\frac{1}{3}\left(\frac{\gamma}{\eta}\right)^3-\frac{1}{3}\xi_2^3-\xi_2^2\left(\Delta_2-\frac{\gamma}{\eta}\right)-\xi_2\left(\Delta_2-\frac{\gamma}{\eta}\right)^2\right]$
5	$\Sigma_{13}+\Sigma_{23}\frac{\gamma}{\eta}+\xi_3$	$\Sigma_{13}\left[\left(\frac{\gamma}{\eta}\right)^2+(1-2\alpha_3+2\xi_3)\left(\frac{\gamma}{\eta}\right)+\xi_3(1-2\alpha_3+\xi_3)+\frac{3(1-2\alpha_3)^2+1}{12}\right]$ $+\Sigma_{23}\left[\frac{1}{3}\left(\frac{\gamma}{\eta}\right)^3+(\xi_3-\alpha_3)\left(\frac{\gamma}{\eta}\right)^2+(\xi_3-\alpha_3)^2\left(\frac{\gamma}{\eta}\right)\right]+\xi_3\alpha_3(\alpha_3-\xi_3)+\frac{1}{3}\xi_3^3$

Note: h=Layer 1 thickness; t=Layer 2 thickness; H=Layer 3 thickness.

$\Sigma_{mn}=\bar{E}_m/\bar{E}_n$, where $m,n=1,2,3$.

$\eta=h/H$, $\gamma=t/H$, $\xi=1/\eta$, $\xi_i=H_i/h$, where $i=1,2,3$.

$\alpha_3=(\eta\xi_3)^2+\Sigma_{23}\gamma(2\eta\xi_3+\gamma)+\Sigma_{13}\eta(2\eta\xi_3+2\gamma+\eta)/2\eta(\eta\xi_3+\Sigma_{23}\gamma+\Sigma_{13}\eta)$.

$\delta=\Sigma_{12}+2\Sigma_{12}\gamma/\eta+(\gamma/\eta)^2/2(\Sigma_{12}+\gamma/\eta)$.

$\Delta_2=\Sigma_{12}(1+2(\gamma/\eta)-2\xi_2)+(\gamma/\eta-\xi_2)^2/2(\Sigma_{12}+(\gamma/\eta)-\xi_2)$.

Shear Debonding Behavior

Fig. 7 shows the typical shear-slip curves generated from the single lap shear fracture tests before and after moisture conditioning. Only the loading curve portion up to the critical state is shown. The unloading portion of the curves could not be consistently reproduced due to the difficulty in monitoring the shear slip response beyond the peak load, at which shear fracture took place in a catastrophic manner.

In general, it is observed that all shear-slip curves were somewhat nonlinear, although the initial portion appeared to be linear before nonlinearity took over. The high-temperature subgroup, regardless of moisture content, exhibited more nonlinearity than the regular temperature subgroup, and was often accompanied by some global yielding signified by the relatively flat portion near the peak load region. Also, shear slip registered for wet specimens just before the critical state was slightly larger than those for the dry ones.

Interface Fracture Toughness

Interface fracture toughness values for both peel and shear fracture cases are computed by means of the specialized fracture energy release rate, G, models developed in parallel with this study (Au 2004; IST 2004) by the writers. By inputting the respective peak loads, the corresponding degraded elastic properties—which were determined from a separate material characterization study—and by choosing the formulation for the particular debonding mode observed—as classified in Fig. 8—the interface fracture toughness values can be obtained from the following expressions:

$$\text{Peel fracture:}\quad \Gamma_{\text{peel}}=\frac{N_{y,\max}^2}{B^2\bar{E}_3h^3}\left(\frac{(\ell+a)^2-\ell^2}{2I_1}+\frac{6\ell^2}{\Sigma_{13}}\right) \tag{1}$$

$$\text{Shear fracture:}\quad \Gamma_{\text{shear}}=\frac{N_{x,\max}^2}{2B^2\bar{E}_3}\left(\frac{1}{A_1h}+\frac{\Psi^2}{I_1h^3}\right) \tag{2}$$

where $N_{y,\max}$=critical peel load; $N_{x,\max}$=critical shear load; B=width of the bond; h=thickness of CFRP; l=cantilever length; a=precrack length; $\bar{E}_3$=degraded plain strain elastic modulus of concrete; Σ_{13}=ratio of plain strain modulus of CFRP to that of concrete; A_1=dimensionless composite area; I_1=dimensionless moment of inertia that contains geometric and material information of the CFRP, epoxy, and concrete layers; and Ψ=eccentricity function. Expressions of A_1 and I_1 for each of the five debonding cases are defined in Table 2. For the details of the derivation, the reader is referred to Au (2004) and IST (2004).

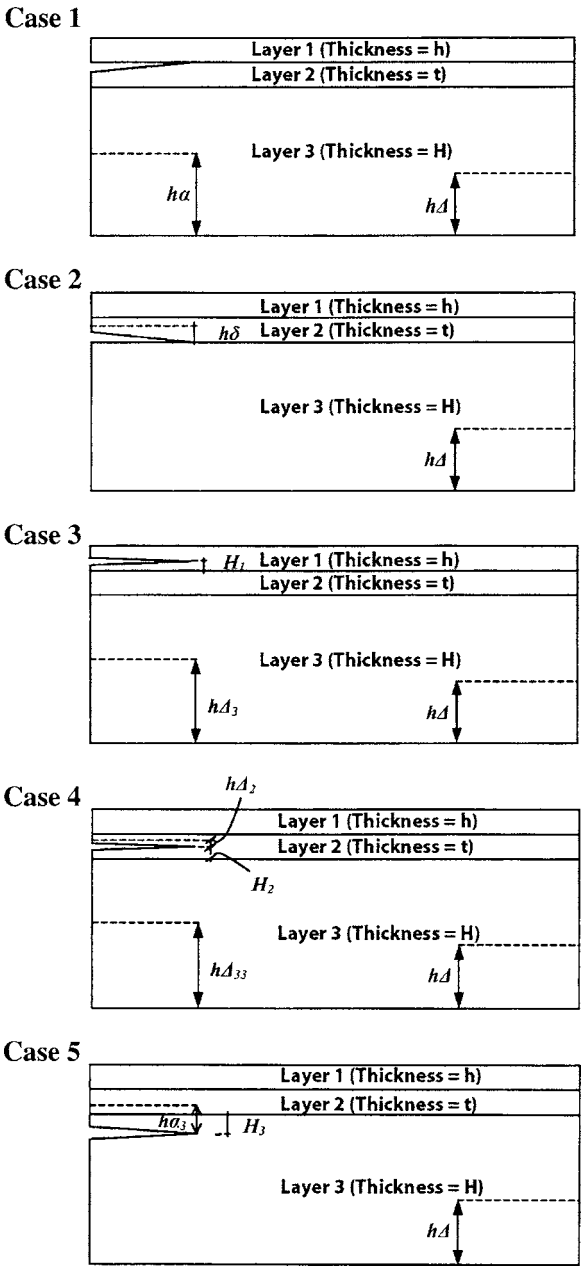

Fig. 8. Idealization and definition of debonding scenarios

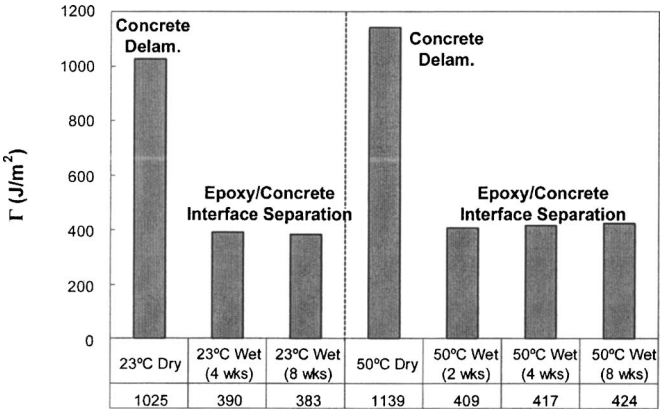

Fig. 9. Peel fracture toughness variations

Peel Fracture Toughness

Average values of peel fracture toughness and their trends with increasing moisture ingress are graphically summarized in Fig. 9, which shows a significant drop in fracture toughness when specimens were moisture conditioned for 2 weeks or more (Test data at 2 weeks for both peel and shear cases with 23 °C could not be obtained due to equipment-related problems). The drop in fracture resistance was more than 60% in both temperature groups. The first-crack fracture toughness then became steady, and did not reduce further with time. Note that the dry fracture toughness represented the peel fracture resistance (that nevertheless consisted of both an open and a shear mode as will be discussed later) of the concrete being used, as the failure modes were unanimously concrete delamination. Note that the fracture toughness of all wet specimens were in the same range, and the readers should recall that the failure modes for all wet specimens were also similar, regardless of the conditioning temperature. Since epoxy/concrete interface separation took place for wet specimens and the fracture toughness values were sharply reduced, it can be suggested that the constituent material limits were not fully (or largely) utilized as concrete did not fracture and epoxy did not craze.

Shear Fracture Toughness

Average values of shear fracture toughness and their trends with increasing moisture ingress are summarized in Fig. 10. It is observed that accelerated moisture diffusion, with the aid of elevated temperature, has resulted in a degradation of more than 50% of the original (dry) shear fracture toughness in as short as 8 weeks, although the reduction slowed down and became more asymptotic starting at the 4-week interval. A similar but slower degradation trend is seen for moisture conditioning without elevated temperature (i.e., 23 °C wet). These degradation trends were considered in line with the peel fracture case when factoring in a similar shift in failure modes.

Discussion

Effect of Moisture on Debonding Resistance

Figs. 9 and 10 indicate that moisture degradation of fracture toughness values is generally observed with prolonged condition-

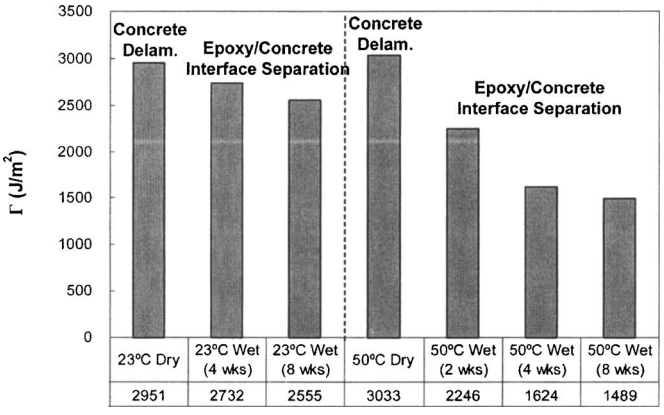

Fig. 10. Shear fracture toughness variations

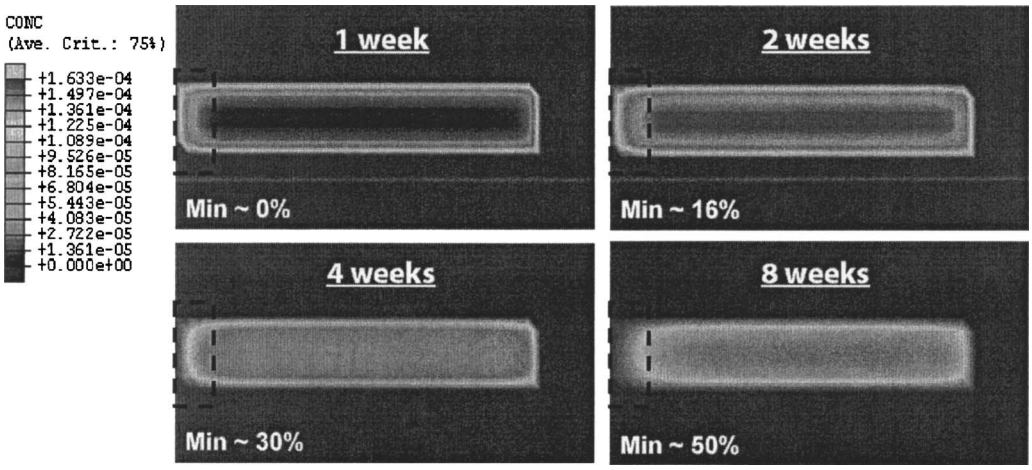

Fig. 11. Moisture concentration profile at the epoxy/concrete interface

ing. This degradation trend is generally common to both temperature groups. The 3D diffusion simulation study indicated that after 8 weeks of continuous moisture conditioning at 50°C, the minimum moisture concentration at the bond interface has reached only 50%. In fact, it was predicted that not until after 200 days would the bond line start to saturate.

In all peel fracture cases, regardless of conditioning environment and duration that was beyond 2 weeks, epoxy/concrete interface separation was observed consistently as the debonding mode in the region where the first crack advance took place. Also, the moisture concentration in that region [as indicated from the dotted lines in Fig. 11, obtained from the finite element moisture diffusion simulation (Au 2004)], that was usually not more than a few centimeters in length, had reached a minimum level of 50%. When the moisture concentration was less than this value, a different debonding mode occurred.

Therefore, a threshold of moisture concentration beyond which no significant further change in mechanism and hence fracture toughness can be implied. In the case herein, that threshold seemed to be 50% or less. The fracture toughness has degraded to a steady value of approximately one-half of the initial value after 8 weeks.

For the shear fracture case, the 3D diffusion simulation study indicated that the entire bond region reached a moisture concentration level of 50% in approximately 8 weeks time, as indicated in Fig. 11. As discussed before, the fracture toughness degradation started to reach an asymptotic value at that time. This observation coincides with that of the peel fracture case where the 50% seemed to be the moisture concentration threshold that would produce little further degradation. In the shear fracture case, however, the duration for such asymptotic behavior was longer because the entire 150 mm bond contributed to the debonding resistance, as opposed to the few centimeters near the edge region in peel fracture.

Further, the shift in debonding mode from concrete delamination to epoxy/concrete interface separation has revealed that when dry, the epoxy/concrete interface fracture toughness was higher than that for concrete delamination, which was approximately 1000 J/m^2, although it would be technically difficult to measure the dry interface toughness values. Nevertheless, that value has dropped to close to 400 J/m^2 after moisture concentration has reached 50% or less, and thus signified a substantial loss of adhesion between the epoxy and concrete as a consequence of moisture ingress.

Effect of Moisture on Locus of Fracture

The locus of fracture for both peel and shear dry cases stayed within the concrete layer. The parent precrack at the epoxy/concrete interface that was generated by an 80-micron thin Teflon film kinked downward into the concrete substrate below the epoxy/concrete interface and subsequent crack propagation stayed close and parallel to that interface, leading to a thin layer of concrete adhered to the debonded strip. The locus of fracture for all wet cases, on the other hand, occurred apparently at the epoxy/concrete interface, staying at the same level as the precrack. In other words, no kinking was observed.

To study the shift in crack kinking behavior, the kink criterion (He and Hutchinson 1989; Büyüköztürk and Lee 1993; Büyüköztürk 1995) is employed. The kink criterion states that when

$$\frac{\Gamma_i}{\Gamma_s} > \frac{G_i}{G^t_{\max}} \tag{3}$$

is satisfied, the parent crack that lies at the interface of two adjoining materials will tend to kink into the substrate in consideration. Here, Γ_i=interface fracture toughness; Γ_s=substrate fracture toughness in Mode I; G_i=interface fracture energy release rate; and $G^t_{\max}$=maximum fracture energy release rate for the kink crack at any putative kink angle. One should note that the ratio is less than unity because G_i is always less than $G^t_{\max}$ due to the definition of $G^t_{\max}$.

Table 3. Dry Fracture Toughness

	Γ_i (J/m^2)	Γ_s (J/m^2)
Dry peel fracture	>1,000	~26
Dry shear fracture	>3,000	~26

Table 4. Numerical G Values and Mode Separation

	G_{peel}, kJ/m^2	G_{shear}, kJ/m^2
Finite element G computation	0.4400 (K^*_{I}=35.58 MPa$\sqrt{\text{mm}}$ K^*_{II}=13.56 MPa$\sqrt{\text{mm}}$)	1.5584 (K^*_{I}=23.99 MPa$\sqrt{\text{mm}}$ K^*_{II}=−67.52 MPa$\sqrt{\text{mm}}$)

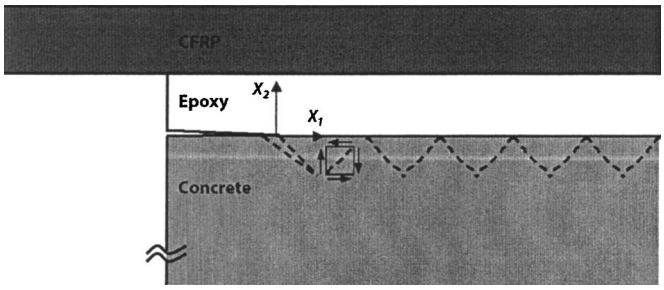

Fig. 12. Effect of negative K_{II}^* on locus of fracture when dry

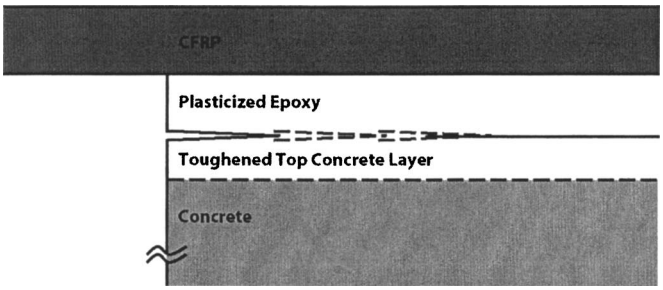

Fig. 13. Effect of moisture plasticization on locus of fracture when wet

Locus of Fracture for Dry Specimens

When dry, the specimens registered a peel and a shear fracture toughness value of roughly 1,000 and 3,000 J/m^2, respectively. Since debonding did not occur at the interface, the actual toughness values of the epoxy/concrete interface were higher than those values. To examine the crack kinking phenomenon, both the Mode I fracture toughness value of concrete (oven dried)—as determined from a separate material characterization study by the writers (Au 2004; IST 2004)—and the interface fracture toughness values are used. The values are summarized in Table 3.

Since $G_i/G_{\max}^t$ has a value less than unity, it is clearly noted that Γ_i/Γ_s is one to two orders of magnitude larger for both the peel case and the shear case. The kink criterion thus predicts that the parent precrack would kink into the concrete substrate. This prediction is in line with the observed failure mode where concrete delamination indeed took place in both loading configurations. The examination also suggests that the Mode I fracture toughness of the epoxy material is higher than 3,000 J/m^2, which is deemed reasonable for an elastomer-toughened epoxy in which substantial crazing can take place.

Although the kink criterion is capable of predicting the initial crack propagation tendency, it fails to provide further insight regarding the subsequent crack front behavior. In other words, the kink criterion explains why the precrack kinked into the concrete substrate, but it does not indicate why the crack continued to propagate close and parallel to the epoxy/concrete interface, but not continue to penetrate deeper into the supposedly brittle concrete block, resulting in a thin layer of concrete adhered to the debonded strip.

To understand this crack propagation behavior, the stress states around the crack tip region need to be understood. As such, a numerical mode-mix separation analysis has been performed on a discretized plain strain fracture model by means of the finite element method and the M-integral analysis (Matos et al. 1989). Using typical material properties and similar load levels as determined from the peel and shear fracture tests, it has been determined that even though the models are subjected to "pure mode" loadings in either the peel or shear case, the mixed mode behavior is profound as indicated by same order K_I^* and K_{II}^*, and Mode I and Mode II stress intensity factors, respectively. Under pure peel and pure shear configurations, and for the computed G values, the corresponding K_I^* and K_{II}^* values are summarized, as examples, in Table 4. Another important observation is that while K_I^*=positive, K_{II}^*=negative. Considering the sign convention of a small element near the epoxy/concrete interface, a negative K_{II}^* value implies crack formation in a fashion that it kinks upward toward the interface, as shown in Fig. 12. Since K_I^*=positive, indicating an opening mode, the upward kinking is facilitated. In other words, once the crack deviates from the precrack location at the epoxy/concrete interface and enters the concrete substrate due to fulfillment of kink criterion as discussed above, the crack will kink back up toward the interface due to the negative K_{II}^* effect. Once that crack tip reaches the interface, the kink criterion is again fulfilled. As a consequence, the crack propagates in a zigzag fashion within the concrete substrate, and tends to stay close to the epoxy/concrete interface due to both the fulfillment of kink criterion and the effect of negative K_{II}^*, resulting in a thin layer of concrete adhering to the debonded strip for all dry cases under both peel and shear fracture configurations.

Table 5. Wet Fracture Toughness

	Γ_i (J/m^2)	Γ_s (J/m^2)
Wet peel fracture	~400	~20
Wet shear fracture	~1,500	~20

Locus of Fracture for Wet Specimens

When wet, all specimens exhibited a consistent interface separation mode at the epoxy/concrete interface. Since the epoxy materials had a Mode I fracture toughness in the very high range, as deduced before, crack kinking was unlikely to occur into the epoxy layer. As such, the kink criterion is implemented to assess the potential of kinking into the concrete substrate. Table 5 summarizes the measured fracture toughness values, with the Mode I substrate fracture toughness being that of wet concrete, as determined again from the separate material characterization study (Au 2004; IST 2004).

Here, although the interface fracture toughness values were greatly reduced by more than one-half, the respective Γ_i/Γ_s ratios still indicate orders of magnitude difference compared to $G_i/G_{\max}^t$, which is practically bounded between zero and unity. In other words, the kink criterion predicts that the interface precrack will kink into the concrete substrate in both cases, which is contrary to the physical observations of an apparent interface separation without evidence of concrete delamination. Since one may not argue with experimental facts and that the kink criterion is not likely to be violated in steady-state fracture (Hutchinson and Suo 1992), the apparent contradiction might be explained by an interfacial material toughening mechanism as a result of plasticization of the penetrated epoxy materials in the top concrete surface.

Structural epoxy is known to plasticize by water (Mays and Hutchinson 1992), which lowers the crosslink density of the polymeric materials that in turn leads to higher fracture toughness values. Since the epoxy has a relatively low viscosity, it is conceivable that it has penetrated into the adjoining surface layer of the porous concrete. As a consequence of moisture ingress in the interface region, the epoxy/concrete mix may have toughened (due to plasticization on the epoxy part) to a point that the

Mode I fracture toughness of this mixture material may have increased to about the same level or even higher than that of the epoxy/concrete interface. In such a case, kinking would not occur and the interface precrack would propagate continuously along that interface until complete debonding took place, as illustrated in Fig. 13. The validity of this behavior requires further material testing of the mixture material for its Mode I fracture toughness and its variation with respect to increasing moisture ingress.

On the other hand, the amount of adhesion between the epoxy and concrete layers has apparently reduced, as indicated by the lower interface fracture toughness and a shift in failure mode when wet. Note that in the dry case, the overall bond fracture toughness values are higher than those of the wet case and yet, the epoxy/concrete interface separation did not occur when dry. This signifies that the dry toughness of the epoxy/concrete interface, which cannot be easily measured, is even higher than the measured values of the dry overall bond fracture toughness, which essentially represent the concrete fracture toughness under a mixed-mode stress state at the crack tip. Thus, the presence of moisture in the interfacial region has led to a substantial degradation of the adhesion between the constituent material layers, contributing in part to the interface separation phenomenon, besides the above-described possible interfacial material toughening mechanism. Thus, it may be stated that the current findings discussed herein point out fundamental behavioral changes in the debonding mechanisms of wet specimens from that of dry specimens. An understanding of exact mechanisms and role of moisture in debonding behavior can be further improved with tests incorporating different epoxy materials and increased test parameters.

Conclusion

The objective of this paper is to develop a new mechanistic understanding of moisture affected debonding failures in CFRP plated concrete systems by means of an interface fracture approach. Central to the investigation is the use of interface fracture toughness as the quantification parameter, which is considered a bond property to analyze, compare, and correlate physical observations of FRP bonded concrete joints. Owing to the nonnegligible epoxy bond line thickness found in real-world retrofitted systems, a newly developed trilayer fracture energy model is used to compute interface fracture toughness values. With this model, the five possible debonding scenarios in FRP bonded concrete, that include interface separation and material decohesion, are quantitatively distinguished and explicitly described.

Debonding characterization is conducted using mesoscale peel and shear fracture models manufactured with full-scale bond lines. These models are subjected to accelerated moisture conditioning to achieve various levels of moisture content in the bond region. They are then mechanically tested at selected time intervals for capturing the change in bond property and debonding mode with respect to increasing moisture concentration, which is evaluated by means of 3D moisture diffusion simulations. Diffusion and mechanical properties of the constituent materials, determined from a separate set of tests in conjunction with the herein investigation, are used as inputs in the diffusion simulation and in the computation of fracture toughness values. The knowledge of computed toughness values, simulated diffusion behavior, and observed debonding modes, combined with finite element fracture computation, mode-mix characterization, and kink criterion implementation, form a synergistic analysis of the mechanistic debonding behavior affected by moisture.

The results have shown that moisture affected debonding is a complex phenomenon that involves physical changes in the bond as well as in its constituent materials. In particular, the fracture toughness can decrease by as much as 60% and become asymptotic upon reaching a certain moisture concentration value, which can be attained in as short as 2 weeks in the case of peel fracture. While concrete delamination mode is observed for dry specimens, the epoxy/concrete interface separation is observed consistently in all wet fracture specimens. Interface fracture analysis indicates that this interfacial debonding mode is attributed to an interfacial material toughening and an interface weakening mechanism as a consequence of moisture diffusion. However, it should also be pointed out that this current study focuses only on one type of epoxy, and that some special epoxies that employ moisture as the curing agent (such as underwater epoxy resins) might result in very different failure modes and interpretations. Yet, the new knowledge and results obtained from this research provide a basis for further analysis and research directions, and the design of FRP bonded concrete systems against moisture affected debonding.

Acknowledgments

This research was supported by the National Science Foundation (NSF) CMS Grant No. 0010126. The writers are grateful to Dr. Perumalsamy N. Balaguru, the cognizant NSF official, for his interest and support in this work. The writers would also like to thank Professor John W. Hutchinson of Harvard University and Professor Ferdinand Rostasy of the Technical University of Braunschweig for their valuable comments and suggestions.

Notation

The following symbols are used in this paper:

$\dot{A}_1$ = normalized composite area;
a = length of precrack;
B = bond width;
E_n = elastic modulus of material layer n;
$\bar{E}_n$ = plain strain elastic modulus of material layer n;
G = fracture energy release rate;
H = thickness of concrete;
H_1 = crack location of Case 3;
H_2 = crack location of Case 4;
H_3 = crack location of Case 5;
h = thickness of FRP;
I_1 = normalized composite moment of inertia;
K_{I}^* = Mode I stress intensity factor for an interface fracture problem;
K_{II}^* = Mode II stress intensity factor for an interface fracture problem;
l = length of FRP laminate cantilever;
$N_{x,\max}$ = critical total constant shear load;
$N_{y,\max}$ = critical total constant peel load;
t = thickness of epoxy layer;

α = normalized neutral axis location of composite Arm 2 for debonding Case 1;
α_3 = normalized neutral axis location of composite Arm 1 for debonding Case 5;
Γ_{peel} = peel fracture toughness;
Γ_{shear} = shear fracture toughness;
γ = thickness ratio between Layers 2 and 3;
Δ = normalized neutral axis location of composite Arm 3 for all debonding cases;
Δ_2 = normalized neutral axis location of composite Arm 1 for debonding Case 4;
Δ_3 = normalized neutral axis location of composite Arm 2 for debonding Case 3;
Δ_{33} = normalized neutral axis location of composite Arm 2 for debonding Case 4;
δ = normalized neutral axis location of composite Arm 1 for debonding Case 2;
η = thickness ratio between Layers 2 and 3;
ν_n = Poisson's ratio of material layer n;
Π = total potential of the bonded system;
Σ_{ij} = elastic modulus ratio between Layers i and j; and
Ψ = eccentricity between the applied and model loading lines.

References

Au, C. (2004). "Moisture degradation in FRP bonded concrete systems: An interface fracture approach," Sc.D. thesis, Massachusetts Institute of Technology, Cambridge, Mass.

Bizindavyi, L., and Neale, K. W. (1999). "Transfer lengths and bond strengths for composites bonded to concrete." *J. Compos. Constr.*, 3(4), 153–160.

Boyajian, D. M., Davalos, J. F., and Ray, I. (2005). "Appraisal of the novel single contoured-cantilever beam." *RILEM Mater. Struct.*, 38, 11–16.

Büyüköztürk, O. (1995). "Fracture mechanics parameters influencing the mechanical properties of concrete composites." *Advanced technology for design and fabrication of composite materials and structures*, G. C. Sih, ed., Kluwer Academic, Boston, 319–331.

Büyüköztürk, O., Gunes, O., and Karaca, E. (2004). "Progress review on understanding debonding problems in reinforced concrete and steel members strengthened using FRP composites." *Constr. Build. Mater.*, 18, 9–19.

Büyüköztürk, O., and Hearing, B. (1998). "Failure behavior of precracked concrete beams retrofitted with FRP." *J. Compos. Constr.*, 2(3), 138–144.

Büyüköztürk, O., and Lee, K. M. (1993). "Assessment of interfacial fracture toughness in concrete composites." *Cem. Concr. Compos.*, 15, 143–151.

Chajes, M. J., Finch, W. W., Januszka, T. F., and Thomson, T. A. (1996). "Bond and force transfer of composite material plates bonded to concrete." *ACI Struct. J.*, 93(2), 208–217.

Chajes, M. J., Thomson, T. A. Jr., and Farschman, C. A. (1995). "Durability of concrete beams externally reinforced with composite fabrics." *Constr. Build. Mater.*, 9(3), 141–148.

Chen, J. F., and Teng, J. G. (2001). "Anchorage strength models for FRP and steel plates bonded to concrete." *J. Struct. Eng.*, 127(7), 784–791.

Gao, B., Kim, J. K., and Leung, C. K. Y. (2003). "Effect of rubber modifier on interlaminar fracture toughness of CFRP-concrete interface." *Compos. Sci. Technol.*, 63, 883–892.

Garden, H. N., and Hollaway, L. C. (1998). "An experimental study of the influence of plate end anchorage of carbon fiber composite plates used to strengthen reinforced concrete beams." *Compos. Struct.*, 42(2), 175–188.

Grace, N. F. (2004). "Concrete repair with CFRP." *Concr. Int.*, 26(5), 45–52.

Gunes, O. (2004). "A fracture based approach to understanding debonding in FRP bonded structural members." PhD thesis, Massachusetts Institute of Technology, Cambridge, Mass.

Hassanen, M. A. H., and Raoof, M. (2001). "Design against premature peeling failure of RC beams with externally bonded steel or FRP plates." *Mag. Concrete Res.*, 53(4), 251–262.

He, M. Y., and Hutchinson, J. W. (1989). "Kinking of crack out of an interface." *J. Appl. Mech.*, 56, 270–278.

Hearing, B. (2000). "Delamination in reinforced concrete retrofitted with fiber reinforced plastics." PhD thesis, Massachusetts Institute of Technology, Cambridge, Mass.

Hutchinson, J. W., and Suo, Z. (1992). "Mixed mode cracking in layered materials." *Adv. Appl. Mech.*, 29, 63–191.

Infrastructure Science and Technology (IST). (2004). "Failure behavior of FRP bonded concrete affected by interface fracture—Part 2." IST Group website ⟨http://web.mit.edu/istgroup/ist/research/projects.htm⟩ (Dec. 1, 2004).

Kaiser, H. P. (1989). "Strengthening of reinforced concrete with epoxy-bonded carbon fibre plastics." Doctoral thesis, Diss. ETH No. 8918, ETH Zurich, Switzerland (in German).

Karbhari, V. M., Engineer, M., and Eckel II, D. A. (1997). "On the durability of composite rehabilitation schemes for concrete: Use of a peel test." *J. Mater. Sci.*, 32(1), 147–156.

Karbhari, V. M., and Zhao, L. (1998). "Issues related to composite plating and environmental exposure effects on composite—Concrete interface in external strengthening." *Compos. Struct.*, 40(3–4), 293–304.

Khalifa, A., Gold, W. J., Nanni, A., and Aziz, A. M. I. (1998). "Contribution of externally bonded FRP to shear capacity of RC flexural members." *J. Compos. Constr.*, 2(4), 195–202.

Khalifa, A., and Nanni, A. (2000). "Improving shear capacity of existing RC T-section beams using CFRP composites." *Cem. Concr. Compos.*, 22, 165–174.

Kimpara, I., Kageyama, K., Suzuki, T., Osawa, I., and Yamaguchi, K. (1999). "Characterization of debonding energy release rate of FRP sheets bonded on mortar and concrete." *Adv. Compos. Mater.*, 8(2), 177–187.

Lorenzis, L. D., Miller, B., and Nanni, A. (2001). "Bond of fiber-reinforced polymer laminates to concrete." *ACI Mater. J.*, 98(3), 356–364.

Matos, P. P. L., McMeeking, R. M., Charalambides, P. G., and Drory, M. D. (1989). "A method for calculating stress intensities in bimaterial fracture." *Int. J. Fract.*, 40, 235–254.

Mays, G. C., and Hutchinson, A. R. (1992). *Adhesives in civil engineering*, Cambridge University Press, Cambridge, U.K.

Meier, U. (1992). "Carbon fiber reinforced polymers, modern materials in bridge engineering." *Struct. Eng. Int. (IABSE, Zurich, Switzerland)*, 2(1), 7–12.

Mukhopadhyaya, P., Swamy, R. N., and Lynsdale, C. J. (1998). "Influence of aggressive exposure conditions on the behavior of adhesive bonded concrete—GFRP joints." *Constr. Build. Mater.*, 12, 427–446.

Nakaba, K., Kanakubo, T., Furuta, T., and Yoshizawa, H. (2001). "Bond behavior between FRP laminates and concrete." *ACI Struct. J.*, 98(3), 359–367.

Neubauer, U., and Rostasy, F. S. (1997). "Design aspects of concrete structures strengthened with externally bonded FRP plates." *Proc., 7th Int. Conf. on Structural Faults and Repair*, Engineering Technics, Edinburgh, Vol. 2, 109–118.

Qiao, P., and Xu, Y. (2004). "Evaluation of fracture energy of composite-concrete bonded interfaces using three-point bend tests." *J. Compos. Constr.*, 8(4), 352–359.

Ritchie, P. A., Thomas, D. A., Lu, L. W., and Connely, G. M. (1991). "External reinforcement of concrete beams using fiberglass reinforced plastics." *ACI Struct. J.*, 88(4), 490–500.

Saadatmanesh, H., and Ehsani, M. R. (1990). "Fiber composites can strengthen beams." *Concr. Int.*, 12(3), 65–71.

Saadatmanesh, H., and Ehsani, M. (1991). "RC beams strengthened with

GFRP plates. I: Experimental study." *J. Struct. Eng.*, 117(11), 3417–3433.
Sharif, A., Al-Sulaimani, G. J., Basunbul, I. A., Baluch, M. H., and Ghaleb, B. N. (1994). "Strengthening of initially loaded reinforced concrete beams using FRP plates." *ACI Struct. J.*, 91(2), 160–168.
Smith, S. T., and Teng, J. G. (2001). "Interfacial stresses in plated beams." *Eng. Struct.*, 23(7), 857–871.
Taljsten, B. (1997). "Strengthening of beams by plate bonding." *J. Mater. Civ. Eng.*, 9(4), 206–212.
Toutanji, H. A., and Gomez, W. (1997). "Durability characteristics of concrete beams externally bonded with FRP composite sheets." *Cem. Concr. Compos.*, 19, 351–358.
Toutanji, H., and Ortiz, G. (2001). "The effect of surface preparation on the bond interface between FRP sheets and concrete members." *Compos. Struct.*, 53, 457–462.
Wan, B., Sutton, M. A., Petrou, M. F., Harries, K. A., and Li, N. (2004). "Investigation of bond between fiber reinforced polymer and concrete undergoing global mixed mode I/II loading." *J. Eng. Mech.*, 130(12), 1467–1475.
Wu, Z., Yuan, H., and Niu, H. (2002). "Stress transfer and fracture propagation in different kinds of adhesive joints." *J. Eng. Mech.*, 128(5), 562–573.